Dynamics of cavitation bubble induced by 193 nm ArF excimer laser in concentrated sodium chloride solutions

Igor Turovets and Daniel Palanker
Laser Center, Hadassah University Hospital, P.O. Box 12000 Jerusalem, 91120, and NanoMed Ltd., Jerusalem, Israel

Yu. Kokotov
Temech Ltd., Jerusalem, Israel

Itzhak Hemo
Department of Ophthalmology, Hadassah University Hospital, Jerusalem, Israel

Aaron Lewis
Laser Center, Hadassah University Hospital, P.O. Box 12000, Jerusalem 91120 and Nanomed Ltd., Jerusalem, Israel

(Received 1 February 1995; accepted for publication 20 November 1995)

Cavitation bubbles were generated by the 193 nm argon fluoride excimer laser delivered with a specially designed tip into absorbing NaCl solution. The dynamics of bubble formation and collapse have been studied using fast flash photomicrography. The bubble dimensions were measured at different time delays as a function of the tip exit diameter, the energy fluence of the laser, and the NaCl concentration. The dynamics of the cavitation bubble created on the tip is compared with the well-studied dynamics of bubbles resulting from dielectric breakdown near a boundary. © *1996 American Institute of Physics.* [S0021-8979(96)02005-6]

INTRODUCTION

Almost all applications of pulsed lasers for ablation, drilling, and cutting of soft tissues in liquid environments are accompanied by the formation of fast-expanding and imploding bubbles.[1–7] These bubbles have been found to determine both the efficiency of the laser treatment and the side effects of the procedure. Side effects caused by such bubble formation include, for example, arterial dilations in angioplasty[2] and damage of the retina during vitreoretinal membrane removal.[4,7] In spite of the major role of bubbles in laser surgery, bubble dynamics has been studied in detail only for mechanisms based on pulsed laser induced dielectric breakdown.

In previous research we have successfully applied the 193 nm laser beam in an absorbing liquid environment for cutting vitreoretinal membranes *in vitro* and *in vivo* at a surprisingly high rate.[1] The ablation depth exceeded a hundred microns per pulse with moderate energy fluences of about 0.2–0.3 J/cm^2/pulse. This result indicated that the mechanism of soft tissue cutting by the ArF excimer laser in a liquid medium differs from ablation mechanism in air.[8] We obtained initial information about this mechanism by investigating the appearance of insoluble and soluble bubbles as a result of irradiation of sodium chloride solutions.[9] These solutions were also used in the present research as models of absorbing substrates because their absorption coefficient could easily be varied over a wide range and because NaCl is a component of all biological liquids.

The aim of the research reported in this article was to study with microsecond time resolution the dynamics of bubbles produced by ArF excimer laser pulses in a highly absorbing liquid environment.

MATERIALS AND METHODS

The ArF excimer laser beam (model LPX 210i excimer laser, Lambda Physik, Gottingen, Germany) was guided through the model 100 EX articulated arm (NanoMed Ltd., Jerusalem, Israel) to a specially designed tip (NanoMed).[1] The exit diameter of the tip varied in the range of 0.15–0.35 mm. The energy delivered through the exit surface of the tip, E, was measured with a model 03 AP-DGX energy meter (Ophir Ltd., Jerusalem, Israel) and varied in the range of 0.05–0.35 mJ/pulse. This corresponds to an energy fluence averaged on the exit surface of the tip in the range of about 0.1–0.5 J/cm^2/pulse. The concentration of absorbing aqueous sodium chloride solutions varied in a range of 0.9–400 g/ℓ.

For visualizing the bubble kinetics a Candela flash-lamp-pumped dye laser with a wavelength of 575 nm and pulse duration of 0.75 μs was guided by a fiber and illuminated a Petri dish held on an inverted microscope stage. Time delay between the excimer and the dye laser pulses varied from 0.5 μs to 100 ms. The microscope was equipped with a computer-controlled charge-coupled device camera PM512A (Photometrics, Tucson, AZ) for imaging of bubble formation and collapse. For measurements of the bubble dimensions at least ten pictures were averaged at each time delay.

RESULTS

At each concentration a cavitation bubble appears after a single pulse when the energy fluence exceeds some threshold. This threshold energy fluence for cavitation bubble formation, F_{thr}, was measured as a function of penetration depth δ [$\delta = 1/(\varepsilon \times C)$], where ε is the NaCl molar absorption coefficient and C is the NaCl molar concentration) (see Fig. 1). F_{thr} is directly proportional to δ (measured in Ref. 9) with

 0021-8979/96/79(5)/2689/5/$10.00

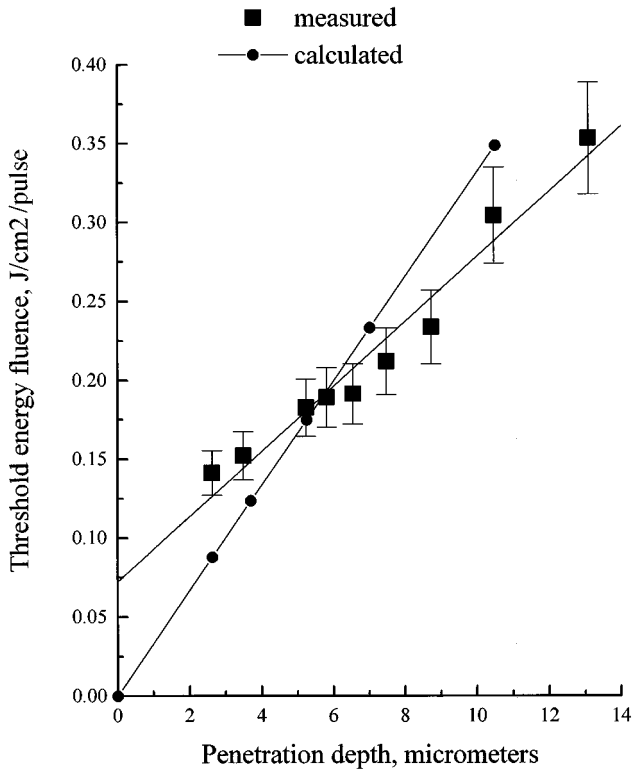

FIG. 1. Dependence of threshold energy fluence for vapor bubble formation on the penetration depth. Exit diamter of the tip was 0.32 mm. Circles present calculated values and squares—measured values.

the coefficient $k_{exp}=206$ mJ/cm^3. For a concentration of 100 g/ℓ that was used in all following experiments F_{thr} is equal to 0.18 J/cm^2/pulse.

Three stages of the process of cavitation bubble appearance were observed in all experiments: growth of the primary bubble, collapse, and "rebound," i.e., secondary bubble formation which is accompanied by movement of the secondary bubble from the tip (see Fig. 2). In the investigated energy fluence range only one collapse stage was observed.

During the growth the bubble was slightly flattened from a spherical configuration at the rear side (the side in contact with the tip). This distortion decreased with increasing the energy fluence of the pulse. The maximal average diameter of the bubble was proportional to the lifetime under all conditions in accordance with the Rayleigh equation.[10] Maximal average bubble volume was studied as a function of the energy exiting from the tip. For an exit diameter of 0.32 mm and sodium chloride concentration of 100 g/ℓ the efficiency of the laser energy conversion to the bubble energy [estimated as the relation of the potential bubble energy to the excess of the laser energy over the threshold energy $(E_{bub}/(E-E_{thr})]$,[14] was 31%.

During the collapse the primary bubble disappears completely in the case when bubble diameter at the maximal expansion stage was smaller than the tip diameter. At higher energy fluence and larger bubbles a rebound stage was observed. At the last stages of collapse a structure consisting of a ring with a central core was produced (see the 55 μs frame

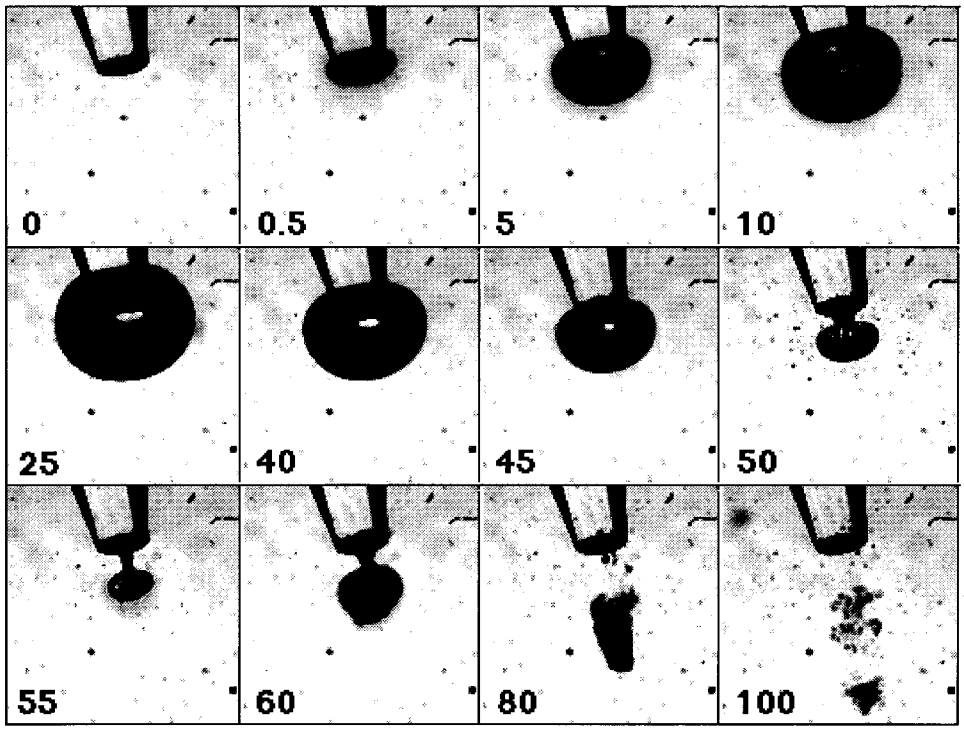

Fig. 2

FIG. 2. Sequence of micrographs of vapor bubble formation and collapse. The laser energy was 0.13 mJ/pulse, the tip exit diameter was 0.24 mm, and the sodium chloride concentration was 100 g/ℓ. The time delay in μs after the laser pulse is shown in the corner of each frame.

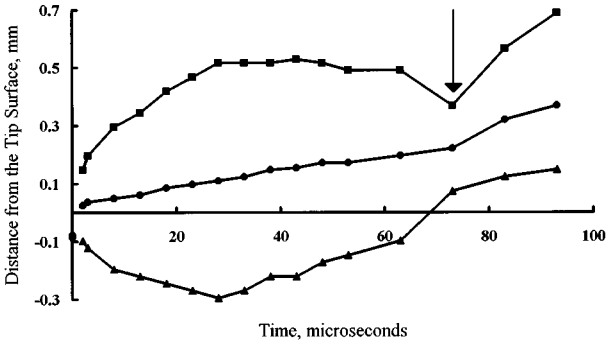

FIG. 3. Distance of front and rear surfaces and of the center of the bubble from the tip exit surface. Sodium chloride concentration was 100 g/ℓ, laser energy was 0.26 mJ/pulse, tip exit diameter was 0.32 mm. Squares present the front surface, circles—the bubble center, and triangles—the rear surface. Arrows indicate the collapse time of the primary bubble.

in Fig. 2). This led to the appearance of a distinctly nonspherical secondary bubble.

In all the experiments the center of the primary bubble moves from the tip with a velocity that depends on the bubble dimension and shape (see Fig. 3). This displacement becomes especially pronounced during the collapse stage because the rear part of the bubble collapses faster than the front. As a result, a rebound always occurs at some distance from the tip surface. After the rebound the nonspherical secondary bubble accelerates in the forward direction and becomes more elongated. The velocity of its center reaches a value of about 7 m/s while the front surface moves even faster. After approximately 30 μs the secondary bubble breaks up leaving many smaller bubbles.

DISCUSSION

The goal of this discussion is to analyze the features of cavitation bubble dynamics resulting from the absorption of the laser beam delivered through the tip. Previously several mechanisms of bubble generation have been suggested for fiber guided laser beams in the wavelength range from 308 nm to 3 μm. All of them are based on evaporation of water due to either direct or indirect heating.

Water itself strongly absorbs radiation of mid-infrared lasers and can be directly evaporated.[3,11] In this case a cavitation bubble forms at the exit surface of the tip. The same process was observed in the case of applications with a 308 nm excimer and dye lasers in strongly absorbing liquids or suspensions.[2,12] When these same lasers were used in transparent media the bubbles were observed on the tissue surface due to tissue heating and subsequent evaporation of intrinsic water[3] or boundary layer water.[13]

Cavitation bubbles have also been observed in various surgical applications of Nd:YAG lasers.[5–7] In this case the medium is transparent to the radiation and the laser beam is focused from outside causing dielectric breakdown. This results in plasma formation and associated evaporation of the surrounding liquid. The dynamics of such bubble formation have been investigated in detail.[5,14–16]

In our model case, when NaCl aqueous solutions are irradiated with the 193 nm ArF laser, the main absorbing substance is chloride anions. It can be argued[9,17] that the principal photochemical process in this system is a result of excitation into a charge-transfer-to-solvent absorption band in which the solvated anion transfers an electron to a water molecule.[17] The next step in the process can either be a thermal degradation to the ground state or the transfer by diffusion of the electron from the hydration sphere of the anion to a hydrogen ion that finally results in hydrogen gas formation.[17] In our previous research[9] it was shown that the quantum yield of such photolysis is always less than 1%, so 99% of the incident laser energy dissipates in solution as heat. A single laser pulse in the investigated energy range is not sufficient for formation of an insoluble hydrogen containing bubble. A train of pulses with an energy fluence beyond the threshold produces a slowly growing insoluble bubble that eventually rises up from the upper side of the tip. The estimated diameter of the insoluble hydrogen gas containing bubble that could be produced at the tip by a single laser pulse did not exceed 110 μm at our maximal energy of 0.35 mJ/pulse.

Cavitation bubbles are formed by the ArF excimer laser by a mechanism in which heat is deposited in water indirectly by the thermal relaxation of the chloride ion from the excited state. A simple estimation could be used[9] to evaluate the temperature rise in NaCl solutions and to calculate the threshold energy fluence for vapor bubble appearance. The threshold energy fluence is proportional to the penetration depth of the radiation with the coefficient k equal to the energy density required for the heating of the boundary layer of the solution to the boiling temperature T_b:

$$F_{\text{thr}}=(T_b-T_0)\times\rho\times c\times\delta=k\times\delta,$$

where $T_0=20$ °C is the initial temperature, c is the heat capacity, ρ is the specific weight, and δ is the penetration depth of the radiation. This model was proved in experiments of van Leeuwen *et al.*,[18] where the threshold energy fluence was found to decrease with increasing the initial temperature to a limit of zero at 100 °C.

For concentrated solutions of NaCl (at $T_0=20$ °C) k is equal to 333 ± 1 J/cm^3 (see Fig. 1). The experimentally measured coefficient $k_{\text{exp}}=206$ J/cm^3 is lower than predicted. This difference can be explained by the beam inhomogeneity: the measured average energy fluence at the exit surface of the tip is lower than the maximal energy fluence which in reality determines the threshold. The extrapolation of the experimental graph to the zero penetration depth results in a value of the threshold mean energy fluence of about 0.072 J/cm^2. This fluence is the measure of the minimal energy that is required for generation of the detectable bubble. Among the components of this minimal energy there are the energy required for evaporation and energy loss through thermal-conductivity.

The dynamics of the cavitation bubble created on the tip is shown schematically in Fig. 4(A). A thin layer of liquid in close proximity to the tip is heated and partially evaporates (line 0). As a result of this evaporation a vapor bubble starts to expand from this layer in all available directions: first in

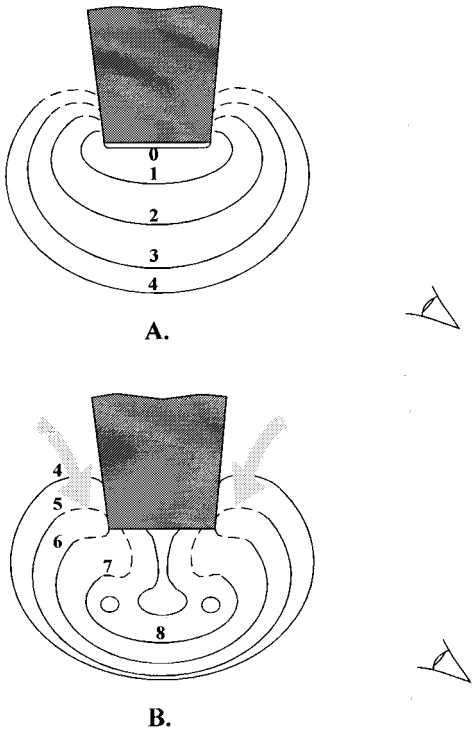

FIG. 4. Scheme of bubble growth (A) and collapse (B) as viewed from the direction of the schematic eye. Laser energy fluence was 0.35 J/cm^2/pulse. Each line presents the section of the bubble at the time $\tau = t/t_{\text{collapse}}$. (0) $\tau < 0.005$, (1) $\tau = 0.009$, (2) 0,09, (3) 0.18, (4) 0.45, (5) 0.73, (6) 0.82, (7) 0.91, (8) 1. The arrows indicate the dominating direction of the water flow.

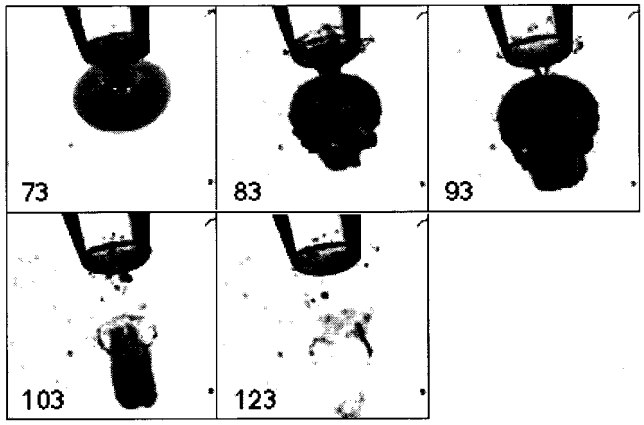

FIG. 5. Sequence of micrographs of secondary vapor bubble formatioin and collapse. Laser energy was 0.26 mJ/pulse, tip exit diameter was 0.32 mm. Sodium chloride concentration was 100 g/ℓ. Time delay after the laser pulse is shown in the corner of each frame.

the forward and the transverse directions relative to the laser beam direction (line 1), and then, as the bubble grows, also in the backward direction. As a result of (1) delay in the backward direction expansion due to geometric constraints, (2) surface tension forces, and (3) the friction of liquid near the tip, the primary bubble has an asymmetrical shape (lines 2–4). The front hemispherical part of the bubble is larger than the rear that has a flattened and distorted shape with a depression around the tip. The influence of the tip and resulting asymmetry decreases with increasing of the bubble size and depends on the energy fluence. Thus, the shape of the growing bubble depends on the energy fluence.

In terms of the collapse, the rear part of the bubble always collapses faster [see Fig. 4(B), line 5] thus resulting in acceleration of the bubble center (lines 6–7). In essence, because of the presence of a depression in the backside of the bubble around the tip a water flow is generated around the tip in the direction of the laser beam [see Fig. 4(B), arrows]. This flow resembles the flow observed during bubble collapses near a boundary.[14] There is one important difference however in our case: the presence of a tip prevents the flow localization and, as a result, restricts a powerful jet formation. The inherent asymmetry of the bubble increases during the collapse and at the last stages a mushroom shape was observed [Fig. 2, 50 μs, Fig. 4(B), line 7, Fig. 5, 73 μs]. This is followed by a structure consisting of an outer gaseous ring and a central gaseous core [Fig. 2, 55 μs and Fig. 4(B) line 8]. The ring has an outer diameter similar to that of the tip and the central core is located between the centers of the tip surface and the ring.

After the last stage of primary bubble collapse a secondary bubble starts to grow. It has an elongated shape (Fig. 2, 60 μs) and moves in the direction of the laser beam. The velocity of the bubble's center is about 7 m/s. Simple estimations of the fluid force imposed on a sphere show that the maximal radius of a spherical bubble that can move in water with such a speed should be less than 30 μm.[19] The larger bubbles should become flattened or even break at such velocity. In contrast, the size of the secondary bubble in our case is about 200 μm (as shown in Figs. 2 and 5). Thus, in order to explain the observed velocity one has to assume that the water flow inflates the bubble in the forward direction thus producing a hollow-tube-like shape with a closed end (Fig. 2, 80 μs and Fig. 5, 83–103 μs).

It seems that the tubelike gaseous body develops from the central core and it is surrounded by the remnants of the gas ring. This stage of the process is clearly seen in Fig. 5, 103 μs. By comparing the frames in Fig. 5 the faster movement of the central core relative to the outer ring is clearly seen.

The different collapse dynamics in our case as compared to the dynamics induced by dielectric breakdown in the vicinity of a boundary results in significant differences in bubble/surface interactions. Bubble collapse near a boundary in the case of dielectric breakdown has the largest damage potential due to the generation of a powerful jet with large amplitudes of pressure that induces considerable damage in tissue.[5] In contrast, a bubble produced at a tip near a tissue surface does not generate such a localized jet, and the pressure amplitude during the collapse will be smaller.

This is true for the cases when the distance from the tip to the surface does not exceed the bubble radius, and for bubbles with diameter comparable to that of the tip. For large symmetrical bubbles generated with a small tip and/or far from the surface of the tissue there can be at least two stages: the first collapse will be similar to that observed in our ex-

periments, but the second one will be closer to the tissue surface and could generate the same cavitation jet observed in dielectric breakdown experiments.[12,14] Thus, the damage potential of the cavitation bubble due to the jet formation is decreased by the influence of the tip and depends on the bubble size and the tip-to-tissue distance. In the case of the ArF excimer laser the maximal exiting energy fluence that the tip can withstand is about 0.5 J/cm^2/pulse. It corresponds to the maximal bubble diameter that is up to 3 times larger than the tip. Thus, in the case of ArF laser the tip will always decrease the jet damage potential. This effect may be very important for medical applications, where minimizing the collateral damage is one of the leading considerations in the choice of a laser system.

CONCLUSIONS

The dynamics of vapor bubbles generated at a tip differs from that of the bubbles created in a dielectric breakdown mechanism near a boundary. In the first case a lack of symmetry of the bubble during the growth phase leads to an asymmetric collapse and to the movement of the primary and the secondary bubble away from the tip. The influence of the tip results in the absence of a powerful localized jet, and this could be advantageous for gentle cutting of biological tissue in liquid environment.

[1] D. Palanker, I. Hemo, I. Turovets, H. Zauberman, and A. Lewis, Invest. Ophthalmol. Vis. Sci. **35**, 3835 (1994).
[2] T. G. van Leeuwen, J. H. Meertence, E. Velema, M. J. Post, and C. Borst, Circulation **87**, 1258 (1993).
[3] T. G. van Leeuwen, L. van Erven, J. H. Meertence, M. Motamedi, M. J. Post, and C. Borst, J. Am. Coll. Cardiol. **19**, 1610 (1992).
[4] T. I. Margolis, D. A. Farnath, M. Destro, and C. A. Puliafito, Arch. Ophthalmol. **107**, 424 (1989).
[5] A. Yogel, P. Schweiger, A. Frieser, M. N. Asiyo, and R. Birngruber, IEEE J. Quantum Electron. **26**, 2240 (1990).
[6] A. Yogel, M. R. C. Capon, M. N. Asiyo-Vogel, and R. Birngruber, Invest. Ophthalmol. Vis. Sci. **35**, 3032 (1994).
[7] C. P. Lin, Y. K. Weaver, R. Birngruber, J. G. Fujimoto, and C. A. Puliafito, Laser Surg. Med. **15**, 44 (1989).
[8] R. Srinivasan and B. Braven, Chem. Rev. **89**, 1303 (1989).
[9] I. Turovets, D. Palanker, and A. Lewis, Photochem. Photobiol. **60**, 412 (1994).
[10] F. R. Young, *Cavitation* (McGraw-Hill, London, 1989), p. 19.
[11] P. E. Dyer, M. E. Khosroshahi, and S. J. Tuft, Appl. Phys. B **56**, 84 (1993).
[12] M. Rudhart and A. Hirth, J. Urol. **152**, 1005 (1994).
[13] K. Rink, G. Delacretaz, and R. S. Salathe, Laser Surg. Med. **16**, 134 (1995).
[14] A. Vogel, W. Lauterborn, and R. Timm, J. Fluid Mech. **206**, 299 (1989).
[15] A. Yogel, S. Busch, K. Jungnickel, and R. Birngruber, Laser Surg. Med. **15**, 32 (1994).
[16] B. Zysset, J. G. Fujimoto, and T. F. Deutsch, Appl. Phys. B **48**, 139 (1989).
[17] M J. Blandamer and M. F. Fox, Chem. Rev. **70**, 59 (1970).
[18] T. G. van Leeuwen, E. D. Jancen, M. Motamedi, A. Welch, and C. Borst, Proc. SPIE **1882**, 13 (1992).
[19] H. Kuchling, *Physik* (VEB Fachbuchverlag, Leipzig, 1980).